Science Bulletin 70 (2025) 2766–2770

Contents lists available at ScienceDirect

Science Bulletin

journal homepage: www.elsevier.com/locate/scib

Short Communication

The rate of magnetic reconnection in non-steady state

Quanming Lu [a,b,c,*], Yukang Shu [a], Cong Chang [d], San Lu [a,b,c], Rongsheng Wang [a,b,c]

[a] CAS Key Lab of Geospace Environment, School of Earth and Space Sciences, University of Science and Technology of China, Hefei 230026, China
[b] CAS Center for Excellence in Comparative Planetology, Deep Space Exploration Laboratory, Hefei 230026, China
[c] Collaborative Innovation Center of Astronautical Science and Technology, Harbin 150001, China
[d] Beijing Institute of Spacecraft System Engineering, Beijing 100094, China

ARTICLE INFO

Article history:
Received 1 December 2024
Received in revised form 30 May 2025
Accepted 3 June 2025
Available online 16 June 2025

In magnetic reconnection, magnetic energy is converted into plasma kinetic energy via the topological rearrangement of magnetic field lines. The reconnection rate, defined as the amount of magnetic flux being reconnected per unit time (or the electric field pointing out of the reconnection plane) at the reconnection site, serves as the primary quantitative measure for predicting the speed of energy conversion in magnetic reconnection. Collisionless magnetic reconnection has attracted significant attention because it can provide a fast reconnection rate, which is around 0.1 when normalized to a properly defined reconnecting magnetic field and Alfvén speed [1,2]. In collisionless magnetic reconnection with the width of the current sheet down to the ion inertial scale, the motions between ions and electrons are decoupled near the X line, which is called the Hall effect, and the diffusion region has a two-layer structure: the electron diffusion region (EDR) and ion diffusion region (IDR) [3,4]. Within the EDR, which spans electron inertial length around the X line, both the ion and electron motions are demagnetized. In the IDR with the spatial scale between the ion and electron inertial lengths around the X line, the ion motions are still demagnetized while the electrons remain frozen in the magnetic field.

The fast reconnection rate in collisionless magnetic reconnection has been considered to be related to the Hall effect for a long time, but the underlying mechanism still remains elusive [5,6]. Recently, Liu et al. [7] developed a theoretical model for the reconnection rate in steady-state collisionless magnetic reconnection. The essence of the model is that the energy conversion in the IDR causes a pressure depletion at the reconnection site, and then the upstream magnetic field develops an opening angle determined by the force-balance condition, enabling the reconnection rate to be of the order 0.1. However, magnetic reconnection is always in a non-steady state, and a dipolarization front (DF) moving toward the downstream is formed due to the pileup of magnetic field from the reconnection site [8,9]. Despite its prevalence in natural systems, the fundamental mechanism governing fast reconnection rates in non-steady regimes remains unexplored. Here, with the help of two-dimensional (2-D) particle-in-cell (PIC) simulations of anti-parallel reconnection, we develop a first-principles theoretical model to explain the reconnection rate in non-steady magnetic reconnection.

A 2-D PIC simulation is performed to study the evolution of magnetic reconnection. The initial equilibrium configuration is a Harris current sheet in the (x, z) plane, and the background plasma density is $n_b = 0.1n_0$ (where n_0 is the peak density of the current sheet). Ions and electrons are assumed to satisfy the Maxwellian distribution with the initial temperature ratio $T_{i0}/T_{e0} = 4$, where $T_{e0}(T_{i0})$ is the initial temperature of electrons (ions). We set the half-width of the current sheet as $\delta = 0.5d_i$(where $d_i = c/\omega_{pi}$ denotes the ion inertial length defined by n_0), the ion-to-electron mass ratio $m_i/m_e = 100$, and $c = 15V_{A0}$(where c denotes the light speed and $V_{A0} = B_0/\sqrt{\mu_0 m_i n_0}$ is the Alfvén speed, and B_0 is the asymptotic magnetic field). The reconnection rate R is normalized by $V_{A0}B_0$. The simulation domain measures $L_x \times L_z = 80d_i \times 20d_i$, with the spatial resolution $\Delta x = \Delta z = 0.05d_i$. The time step is $\boldsymbol{\Omega}_i \Delta t = 0.001$ (where $\boldsymbol{\Omega}_i = eB_0/m_i$ is the ion gyrofrequency). Periodic boundary condition is assumed in the x direction, while in the z direction, we use conducting boundary conditions. The system evolves spontaneously without artificial initial perturbations.

While two X-lines emerge simultaneously in the simulation domain, our analysis focuses exclusively on one. The characteristics around the selected X line are displayed in Fig. 1. The recon-

* Corresponding author.
E-mail address: qmlu@ustc.edu.cn (Q. Lu).

https://doi.org/10.1016/j.scib.2025.06.014

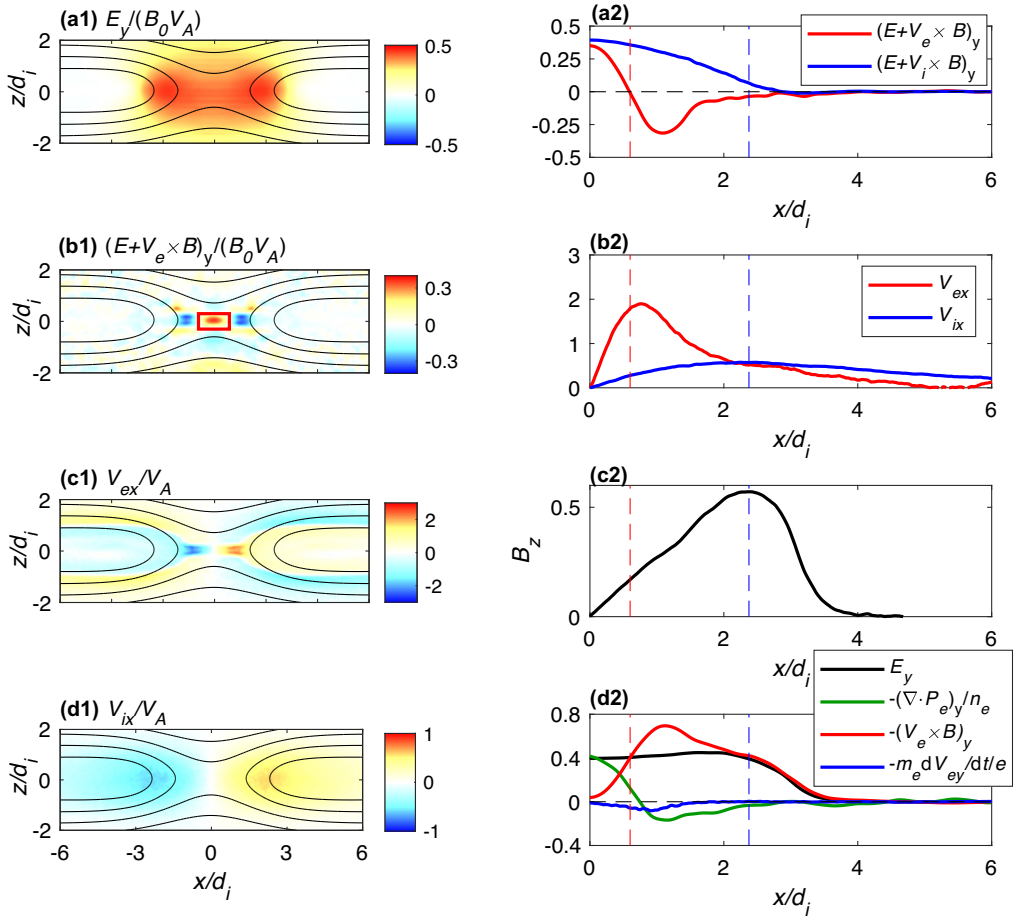

Fig. 1. The distribution of physical parameters around the selected X line at $\Omega_i t = 41.5$. (a1) The reconnection electric field E_y. (b1) The nonideal electric field $(\boldsymbol{E}+\boldsymbol{V}_e\times\boldsymbol{B})_y$, here the region with $(\boldsymbol{E}+\boldsymbol{V}_e\times\boldsymbol{B})_y>0$ is the inner EDR, which is circled by a red box. (c1) The electron outflow velocity V_{ex}. (d1) The ion outflow velocity V_{ix}. (a2) The profiles of $(\boldsymbol{E}+\boldsymbol{V}_e\times\boldsymbol{B})_y$ and $(\boldsymbol{E}+\boldsymbol{V}_i\times\boldsymbol{B})_y$ along the line $z=0$. (b2) The profiles of electron outflow velocity V_{ex} and ion outflow velocity V_{ix} along the line $z=0$. (c2) The profile of magnetic field B_z along the line $z=0$. (d2) The reconnection electric field E_y, the convective electric field term $-(\boldsymbol{V}_e\times\boldsymbol{B})_y$, the electron pressure divergence term $-(\nabla\cdot\vec{\boldsymbol{P}}_e)_y/n_e$, the electron inertia term $((-m_e/e)(dV_{ey}/dt))$ along the line $z=0$. The red and blue vertical dashed line in (a2–d2) denotes the just downstream of the EDR and IDR.

nection electric field is produced in the vicinity of the X line (Fig. 1a1). The EDR features a two-layer structure characterized by nonzero nonideal electric fields $(\boldsymbol{E}+\boldsymbol{V}_e\times\boldsymbol{B})_y$: the inner EDR with $(\boldsymbol{E}+\boldsymbol{V}_e\times\boldsymbol{B})_y>0$ around the X line, and the outer EDR with $(\boldsymbol{E}+\boldsymbol{V}_e\times\boldsymbol{B})_y<0$ in the downstream of the inner EDR (Fig. 1b1 and a2) [10,11]. Here, the inner EDR is actually the EDR described in the standard model of collisionless magnetic reconnection. Downstream of the outer EDR, the magnetic field is piled up, and a pair of DFs subsequently forms (Fig. 1c2). When the electrons move away from the X line, their outflow speed increases in the inner EDR, and peaks in the outer EDR (Fig. 1c1 and b2). The ion outflow speed increases slowly when they move away from the X line, and the peak value is located around the DF (Fig. 1d1 and b2). Around the DF region, the ion and electron motions are coupled together and frozen in with the magnetic field, and their outflow speeds are almost the same [12]. The DF can be considered as the downstream boundary of IDR (Fig. 1a2 and c2). In this paper, if there is no explicit statement, the EDR refers to the inner EDR. According to the generalized Ohm's law, the electric field in the EDR can be expressed as $\boldsymbol{E}\approx-\boldsymbol{V}_e\times\boldsymbol{B}-\nabla\cdot\vec{\boldsymbol{P}}_e/(en_e)-(m_e/e)(d\boldsymbol{V}_e/dt)$, and the terms on the right-hand side are the convective electric field term, electron pressure divergence term, and electron inertia term, respectively. The reconnection electric field at the center of the EDR is dominated by the electron pressure divergence term, while that around just downstream of the EDR is contributed mainly by the convective electric field term (Fig. 1d2). The electron inertia term is negligible compared with the other terms.

Magnetic reconnection experiences non-steady evolution (Movie S1 and Fig. S1 online), and the reconnection rate $R=E_{yX}/(V_{A0}B_0)$ (the reconnection electric field at the X line normalized by $V_{A0}B_0$) also changes with time. As shown in Fig. 2a, the evolution can be separated into two stages. During stage I ($\boldsymbol{\Omega}_i t$ = 35–43.5), the reconnection rate undergoes rapid enhancement, and it reaches the peak value 0.40 at about $\boldsymbol{\Omega}_i t$ = 43.5. In the second stage (Stage II), the reconnection rate R decreases gradually from about $\boldsymbol{\Omega}_i t$ = 43.5. The reconnection electric field just downstream of the EDR can be expressed as $E_{yE}=V_{exE}B_{zE}$ (where V_{exE} and B_{zE} are the electron outflow speed V_{ex} and magnetic field B_z just downstream of the EDR). Around the DF, both the ions and electrons become magnetized, and the reconnection electric field is $E_{yI}=V_{ixI}B_{zI}$ (where V_{ixI} and B_{zI} are the ion outflow speed V_{ix} and magnetic field B_z around the DF. Please note that the electron outflow speed V_{ex} is almost the same as the ion outflow speed V_{ix} around the DF, that is $V_{ixI}\approx V_{exI}$). E_{yE} is almost the same as the reconnection electric field in the X line, and an obvious difference between E_{yI} and E_{yX} appears at about $\boldsymbol{\Omega}_i t$ = 42 and then becomes larger and larger. The length of the IDR increases slowly in Stage

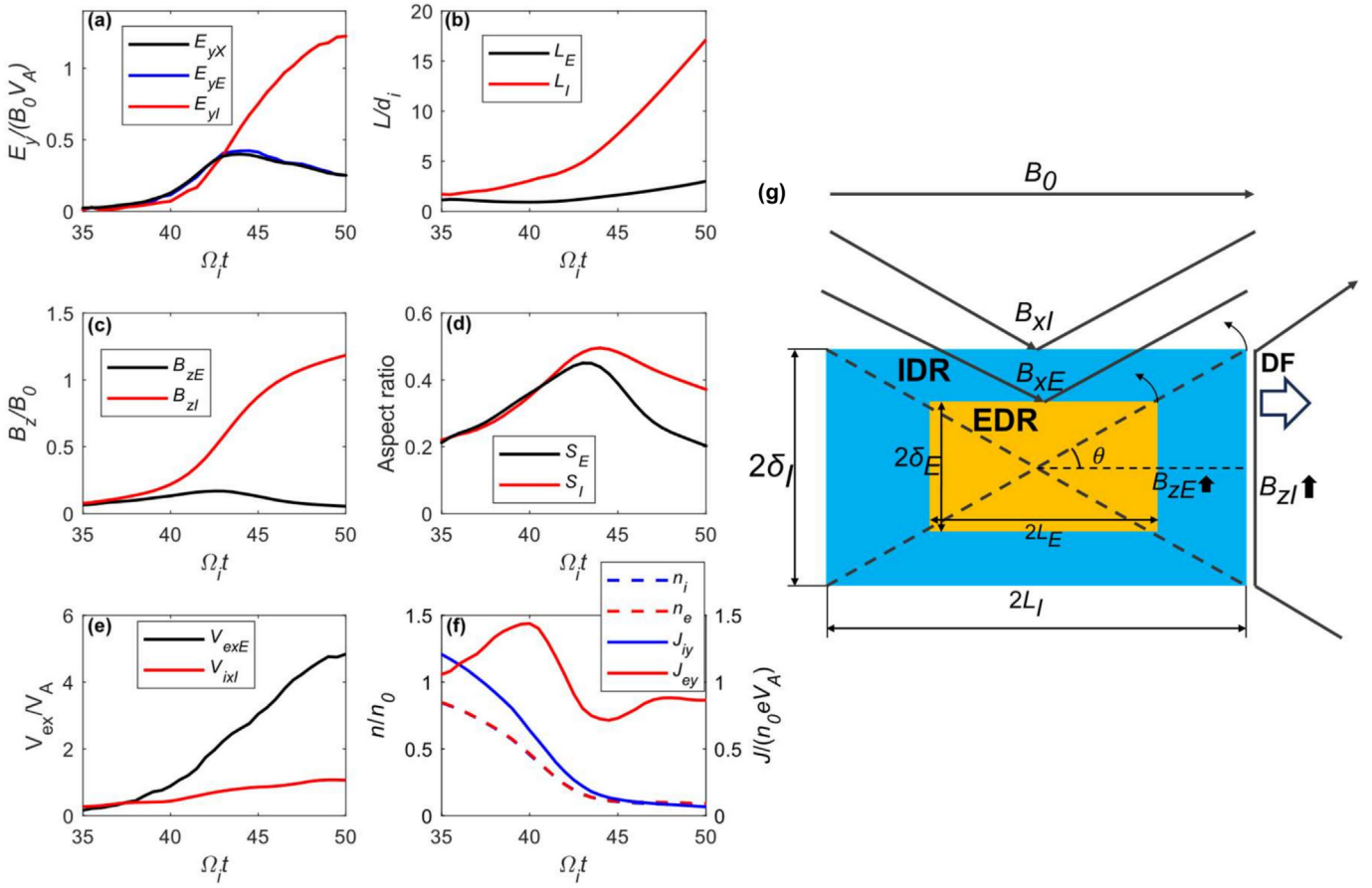

Fig. 2. The evolution of physical parameters around the selected X line. (a) The reconnection electric field at the X line (E_{yX}), at the just downstream of the EDR (E_{yE}), and at the just downstream of the IDR (E_{yI}). (b) The half-length of the EDR (L_E), and half-length of the IDR (L_I). (c) The magnetic field just downstream of the IDR (B_{zE}), and that just downstream of the IDR (B_{zI}). (d) The aspect of the EDR $S_E = \delta_E/L_E$ (where δ_E is the half-width of the EDR), and the aspect of the IDR $S_I = \delta_I/L_I$ (where δ_I is the half-width of the IDR). (e) The electron outflow speed just downstream of the EDR (V_{exE}), and the ion outflow speed just downstream of the IDR V_{ixI}. (f) The average values of the ion number density (n_i), the electron density (n_e), the ion current density (j_{iy}), and electron current density (j_{ey}) in the EDR. (g) Diagram of the EDR and IDR. B_0 is the asymptotic magnetic field of the current sheet, B_{xI} and B_{xE} are the magnetic fields just upstream of the IDR and EDR, B_{zI} and B_{zE} are the magnetic fields just downstream of the IDR and EDR, δ_I and δ_E are the half-widths of the IDR and EDR, L_I and n are the half-lengths of the IDR and EDR.

I, and downstream expansion accelerates significantly during Stage II. The length of the EDR almost does not change in Stage I, and it then begins to increase in Stage II (Fig. 2b). During magnetic reconnection, the magnetic flux is transferred from the upstream into the downstream through the X line, therefore, we can observe the enhancement of the magnetic field B_z in the downstream. However, the magnetic field B_z just downstream of the EDR begins to decrease in Stage II because of the expansion of the EDR toward the downstream, while the magnetic field B_z of the DF increases rapidly in Stage II (Fig. 2c). The aspect ratios of both the EDR and IDR increase in Stage I and then decrease in Stage II, and in Stage I they are almost the same because of the straightening out of magnetic field lines by the magnetic tension (Fig. 2d). The electron outflow speed from the EDR V_{exE} and the ion (electron) outflow speed from the IDR $V_{ixI} \approx V_{exI}$ at first experiences an increase and then saturates at about $\boldsymbol{\Omega}_i t$ = 48, and their maximum values are about 5.0 and 1.0 V_A, respectively (Fig. 2e). Fig. 2f shows the evolution of the plasma and current densities in the EDR. The electron and ion density in inner EDR is almost the same, and they decrease rapidly until about 0.1 n_0 in Stage I, which is almost the same as the background plasma density of the Harris current sheet. This leads to the same trend for the evolution of the ion current density in the inner EDR. Because the electrons in the EDR are easy to be accelerated by the reconnection electric field, the electron current density at first increases, and then decreases after the electrons move away from the EDR. However, a striking current disparity emerges after about $\boldsymbol{\Omega}_i t$ = 40, with electron current densities surpassing ion values by an order of magnitude. Based on these characteristics, we can plot the diagram of the electron and ion diffusion regions for theoretical modelling (Fig. 2g).

The scale of the reconnection electric field at the center of the EDR, which is dominated by the electron pressure divergence term, is determined by the trapping length of electrons in a field reversal. Their characteristic lengths in the x and z directions can be expressed as $\lambda_x = \left[\frac{2m_eT_e}{e^2\left(\frac{\partial B_z}{\partial x}\right)^2}\right]^{1/4}$ and $\lambda_z = \left[\frac{2m_eT_e}{e^2\left(\frac{\partial B_x}{\partial z}\right)^2}\right]^{1/4}$ (where T_e is the electron temperature) [13]. In our simulation, the trapping length of electrons is smaller than that of the EDR. Therefore, the region where the electron pressure tensor term dominates is limited to the center of the EDR, and the reconnection electric field can be described as $E_{yX} \approx \frac{1}{e}\frac{\partial V_{ex}}{\partial x}\sqrt{2m_eT_e}$[3]. The reconnection electric field accelerates the electrons around the X line in the y direction, and then the electron current density in the y direction increases. At the X line, the only force acting on the electrons is the electric field force, and the electron motions can be described as $d|V_{eyX}|/dt \propto |E_{yX}| \propto |V_{exE}|$. When leaving away from the X line, the electrons perform meandering motions, their outflow speed $|V_{exE}|$ should be proportional to $|V_{eyX}|$. At last, we can get $d|V_{eyX}|/dt \propto |V_{eyX}|$. Therefore, the reconnection electric field at the

center of the EDR experiences a self-reinforcing process, and grows rapidly over time [14].

The reconnection electric field at the X line is almost the same as that in the just downstream of the EDR, and we will use the latter one ($E_{yE} = V_{exE}B_{zE}$) to investigate the evolution of the reconnection rate R in Stage I, where $S_L \approx S_{LE} \approx S_{LI}$. Because the downstream boundary of the EDR moves slowly, the time derivation of the electron outflow velocity is negligible [12]. The x component of the electron momentum equation along the line $z = 0$ can be described as the follow

$$n_e m_e V_{ex}\frac{\partial V_{ex}}{\partial x} \approx -en_e\left(E_x + V_{ey}B_z\right) - \frac{\partial P_{exx}}{\partial x}. \tag{1}$$

The contribution of Lorentz force ($-en_eV_{ey}B_z$) is dominated in the EDR, and we neglects the contributions of the Hall electric field ($-en_eE_x$) and electron pressure ($-\partial P_{exx}/\partial x$)(Fig. S2 online) [12]. Therefore, in the just downstream of the EDR the equation can be written as

$$n_e m_e V_{ex}\frac{\partial V_{ex}}{\partial x} \approx j_{ey}B_z. \tag{2}$$

According to $\nabla \times \boldsymbol{B} = \mu_0\boldsymbol{J}$, we can get $(\frac{\partial B_x}{\partial z} - \frac{\partial B_z}{\partial x}) \approx \mu_0(j_{ey} + j_{iy})$. With the growth of the reconnection electric field at the center of the EDR, the electron outflow speed V_{ex} from the X line increases, and the magnetic field B_z is accumulated just downstream of the EDR. It leads to the decrease of current density $j_y = j_{ey} + j_{iy}$ in the EDR. As shown in Fig. 2f, the decrease of the ion current density is much faster than that of the electron current density. When the reconnection rate approaches the maximum value (around $\boldsymbol{\Omega}_i t$ = 43.5), the electron current density is much larger than the ion current density $j_{ey} \gg j_{iy}$. Therefore, $j_{ey} \approx \frac{1}{\mu_0}\frac{B_{xE}}{\delta_E}\left(1 - \frac{\delta_E^2}{L_E^2}\right)$. Because the magnetic field lines threading the X-line are approximately straight in Stage I, and we have $S_L \approx \frac{\delta_E}{L_E} \approx \frac{\delta_I}{L_I}$. The electron outflow speed is

$$V_{exE} \approx V_{Ae}\left(1 - S_L^2\right)^{1/2}. \tag{3}$$

When the reconnection rate approaches the maximum value, the plasma density is nearly uniform in the diffusion regions, which is about the same as that of the background plasma of the Harris current sheet (n_b) (Fig. S3 online), that is $n_e \approx n_b$ and $V_{Ae} = \frac{B_{xE}}{\sqrt{\mu_0 n_b m_e}}$. The plasma is nearly incompressible, therefore, $V_{izI}L_I \approx V_{ixI}\delta_I$ and $V_{ezE}L_E \approx V_{exE}\delta_E$. The reconnection electric field is uniform in the inflow region, $V_{izI}B_{xI} \approx V_{ezE}B_{xE}$. Based on these, we can obtain

$$\frac{B_{xE}}{B_{xI}} \approx \frac{V_{ixI}}{V_{exE}}. \tag{4}$$

We assume that the profile of the plasma pressure in the outflow direction is nearly uniform, and the pressure gradient force is small compared to the magnetic tension force. The ion outflow speed just downstream of the IDR is $V_{ixI} \approx V_{Ai}\left(1 - S_L^2\right)^{\frac{1}{2}}$, where $V_{Ai} = \frac{B_{xI}}{\sqrt{\mu_0 n_b m_i}}$[5]. Then

$$\frac{V_{ixI}}{V_{exE}} \approx \frac{B_{xI}}{B_{xE}}\sqrt{\frac{m_e}{m_i}}. \tag{5}$$

According to Eqs. (4) and (5), the following equation can be obtained

$$\frac{B_{xE}}{B_{xI}} \approx \left(\frac{m_e}{m_i}\right)^{1/4}. \tag{6}$$

In the upstream of the IDR, the inward-directed magnetic pressure gradient force is balanced by the outward -directed magnetic tension[5], we have

$$\frac{B_{xI}}{B_0} \approx \frac{1 - S_L^2}{1 + S_L^2}. \tag{7}$$

Combing Eqs. (6) and (7), the reconnection electric field in the EDR ($E_{yE} = V_{exE}B_{zE}$) can be expressed as

$$\begin{aligned} E_{yE} &\approx S_L B_{xE} V_{Ae}\left(1 - S_L^2\right)^{1/2} \\ &\approx \left(\frac{n_0}{n_b}\right)^{1/2} S_L\left(\frac{1 - S_L^2}{1 + S_L^2}\right)^2\sqrt{1 - S_L^2}B_0 V_{A0}. \end{aligned} \tag{8}$$

At last, the reconnection rate reaches its peak value R_{peak} when the aspect ratio is S_{Lp}, then

$$R_{peak} \approx \left(\frac{n_0}{n_b}\right)^{1/2} S_{Lp}\left(\frac{1 - S_{Lp}^2}{1 + S_{Lp}^2}\right)^2\sqrt{1 - S_{Lp}^2}. \tag{9}$$

The peak reconnection rate R_{peak} is determined by n_0/n_b and the aspect ratio S_{Lp}, while remaining independent of the ion-to-electron mass ratio. From Fig. S4 (online), which shows the variation of $F = S_L\left(\frac{1-S_L^2}{1+S_L^2}\right)^2\sqrt{1 - S_L^2}$ as a function of S_L, we can know that the maximum value of F is $F_{max} \approx 0.20$ at the aspect ratio $S_{Lmax} \approx 0.34$. If S_{Lp} can reach up to S_{Lmax}, the peak reconnection rate during the evolution of non-steady reconnection is $R_{peak} \approx 0.64$ based on Eq. (9), whereas our simulation yields $R_{peak} \approx 0.40$ at $S_{Lp} \approx 0.44$. This discrepancy likely originates from neglected plasma pressure and ion current contributions within the EDR. From Fig. 2, we can also find that the aspect ratio S_L increases until the reconnection rate R reaches its peak value, where the aspect ratio S_{Lp} is close to S_{Lmax}. We have also run cases with different values of n_0/n_b, and the evolution of the aspect ratio S_L and reconnection rate R is the same. Therefore, it is reasonable to assume that with the increase of the open angle of the EDR during non-steady reconnection, the peak reconnection rate R will at last reach the value $(n_0/n_b)^{1/2}F_{max}$.

We proposed a first-principles theory of the reconnection rate during non-steady magnetic reconnection in Harris-type current sheets. Based on 2D PIC simulations, we find that the reconnection electric field at the X line can be well represented by that just downstream of the EDR, where the electrons are magnetized. The reconnection electric field around the X line is dominated by the electron pressure tensor term, and it experiences a self-reinforcing process, which leads to a rapid increase in the electron outflow speed from the X line with time. When these electrons reach just downstream of the EDR, they are magnetized. Their outflow speed is limited by the Lorentz force, which depends on the opening angle of the EDR. The magnetic field is piled up downstream of the EDR, and the opening angle is then enhanced until the reconnection rate reaches a peak value. The peak value of the reconnection rate is on the order of 0.1.

Our model also predicts that the peak reconnection rate is proportional to $\sqrt{n_0/n_b}$, while it is independent of the ion-to-electron mass ratio. The relation between the peak reconnection rate and n_b/n_0 obtained in simulations is consistent with the prediction based on Eq. (9) (Fig. S5 online). At the same time, the mass-ratio independence aligns with previous kinetic simulations [15]. It should be noted that choosing different definitions of the Alfvén speed can change the expression of the reconnection rate. The Alfvén speed in our paper is defined as $V_{A0} = B_0/\sqrt{\mu_0 m_i n_0}$, which is based on the initial peak density of the current sheet n_0. This definition yields our derivation of Eq. (9). When adopting the upstream plasma density n_b to define the Alfvén speed as $V_{Ab} = B_0/\sqrt{\mu_0 m_i n_b}$, the expression of the reconnection rate trans-

forms to $E_{yX}/V_{Ab}B_0 \approx S_L\left(\frac{1-S_L^2}{1+S_L^2}\right)^2\sqrt{1-S_L^2}$. With this definition, the peak reconnection rate yields about 0.20. This dependency highlights the critical importance of choosing normalization parameters, particularly for *in-situ* satellite diagnostics where global measurements are inherently unavailable.

Conflict of interest

The authors declare that they have no conflict of interest.

Acknowledgments

This work was supported by the National Key Research and Development Program of China (2022YFA1604600) and the National Natural Science Foundation of China (42174181).

Author contributions

Quanming Lu conceived the idea, oversaw the project, and wrote the manuscript. Yukang Shu and Cong Chang performed the simulations. San Lu and Rongsheng Wang contributed to the interpretation of the simulation results. All of the authors discussed the results and commented on the paper.

Appendix A. Supplementary material

Supplementary data to this article can be found online at https://doi.org/10.1016/j.scib.2025.06.014.

References

[1] Shay MA, Drake JF, Rogers BN, et al. The scaling of collisionless, magnetic reconnect ion for large systems. Geophys Res Lett 1999;26:2163–6.
[2] Phan TD, Sonnerup BUÖ, Lin RP. Fluid and kinetics signatures of reconnection at the dawn tail magnetopause: wind observations. J Geophys Res Space Phys 2001;106:25489–501.
[3] Hesse M, Schindler K, Birn J, et al. The diffusion region in collisionless magnetic reconnection. Phys Plasmas 1999;6:1781–95.
[4] Pritchett PL. Geospace environment modeling magnetic reconnection challenge: simulations with a full particle electromagnetic code. J Geophys Res Space Phys 2001;106:3783–98.
[5] Liu YH, Hesse M, Guo F, et al. Why does steady-state magnetic reconnection have a maximum local rate of order 0.1? Phys Rev Lett 2017;118:085101.
[6] Cassak PA, Liu YH, Shay MA. A review of the 0.1 reconnection rate problem. J Plasma Phys 2017;83:1–17.
[7] Liu YH, Cassak P, Li XC, et al. First-principles theory of the rate of magnetic reconnection in magnetospheric and solar plasmas. Commun Phys 2022;5:97.
[8] Runov A, Angelopoulos V, Sitnov MI, et al. THEMIS observations of an earthward-propagating dipolarization front. Geophys Res Lett 2009;36:1–7.
[9] Sitnov MI, Swisdak M, Divin AV. Dipolarization fronts as a signature of transient reconnection in the magnetotail. J Geophys Res Space Phys 2009;114:2008JA013980.
[10] Shay MA, Drake JF, Swisdak M. Two-scale structure of the electron dissipation region during collisionless magnetic reconnection. Phys Rev Lett 2007;99:155002.
[11] Tian ZC, Zhou M, Man HY, et al. Simultaneous observation of the inner and outer electron diffusion region in reconnection with larger guide field. Astrophys J 2023;957:42.
[12] Chang C, Lu QM, Lu S, et al. Ion and electron motions in the outer electron diffusion region of collisionless magnetic reconnection. Earth Planet Phys 2024;8:472–8.
[13] Biskamp D, Schindler K. Instability of two-dimensional collisionless plasmas with neutral points. Plasma Phys 1971;13:1013–26.
[14] Lu QM, Lu S, Huang C, et al. Self-reinforcing process of the reconnection electric field in the electron diffusion region and onset of collisionless magnetic reconnection. Plasma Phys Control Fusion 2013;55:085019.
[15] Shay MA, Drake JF. The role of electron dissipation on the rate of collisionless magnetic reconnection. Geophys Res Lett 1998;25:3759–62.